ELSEVIER

NeuroImage

www.elsevier.com/locate/ynimg
NeuroImage 24 (2005) 635–645

In vivo detection limits of magnetically labeled embryonic stem cells in the rat brain using high-field (17.6 T) magnetic resonance imaging

Albrecht Stroh,[a,*,1] Cornelius Faber,[b,1] Thomas Neuberger,[b] Peer Lorenz,[c] Katharina Sieland,[a] Peter M. Jakob,[b] Andrew Webb,[b] Herbert Pilgrimm,[d] Ralf Schober,[e] Elena E. Pohl,[f] and Claus Zimmer[a,g]

[a]*Department of Radiology and Neuroradiology, Charité University Hospital, Berlin, Germany*
[b]*Department of Physics, EP5, University of Würzburg, Germany*
[c]*Department of Pharmacology and Toxicology, Charité University Hospital, Berlin, Germany*
[d]*Ferropharm GmbH, Teltow, Germany*
[e]*Department of Neuropathology, University Hospital Leipzig, Germany*
[f]*Neuroscience Research Center, Charité University Hospital, Berlin, Germany*
[g]*Department of Neuroradiology, University Hospital Leipzig, Germany*

Received 17 February 2004; revised 18 June 2004; accepted 10 September 2004
Available online 24 November 2004

Stem cell transplantation is a promising therapeutic approach for several neurological disorders. However, it has yet to fulfill its high expectations, partially due to the lack of a reliable noninvasive method for monitoring the biodistribution of the grafted stem cells in vivo. We have used high-resolution magnetic resonance imaging (MRI) at 17.6 T, combined with efficient magnetic labeling of the stem cells with iron oxide nanoparticles, in order to assess the in vivo detection limit in small animal models. Injection of different concentrations of magnetically labeled stem cells in gel phantoms led to significant reductions in image intensity from small cellular clusters of less than 10 cells. To determine the detection limit in vivo, various numbers of both labeled and unlabeled cells were injected stereotactically into the striatum of rats. Significant hypointense signal changes were observed for 100 labeled cells. After injection of approximately 20 labeled cells, signal reduction at the injection site was observed but could not be assigned unambiguously to the cells. Our results show that high-field MRI allows tracking of a minimal number of cells in vivo, well below the number used in previous studies, opening the possibility of gaining new insights into cell migration and differentiation.

Keywords: Stem cells; MR imaging; Molecular imaging; Magnetic cell labeling

Introduction

The potential of stem or progenitor cells to regenerate damaged tissue in neuronal diseases has attracted much attention in neurological research over recent years. Stem cell transplantation is a promising therapeutic approach for Parkinson disease (Bjorklund et al., 2002; Isacson et al., 2003; Sun et al., 2003), cerebral ischemia, and chronic neuroinflammation (Ben Hur et al., 2003; Bulte et al., 2003; Fukunaga et al., 1999; Modo et al., 2002b; Pluchino et al., 2003). However, clinical studies concerning long-term survival, differentiation, and migration of grafted cells in the host organism have been not very effective (Check, 2003; Eskandar et al., 2003), because no reliable noninvasive method exists for monitoring transplanted cells in vivo at high spatial resolution over an extended period of time. Positron emission tomography (PET) (Lindvall et al., 1994) allows noninvasive detection with very high sensitivity but suffers from poor spatial resolution. Magnetic resonance imaging (MRI) can provide images with very high spatial resolution in small animals but requires efficient labeling of the cells for these to be observed. Several strategies to make cells MR-visible have been developed. Most efforts incorporate small iron oxide particles into cells which leads to a strong decrease in the transverse relaxation time of water protons diffusing close to the cells, resulting in turn in signal loss in T_2^*-weighted gradient echo images (Arbab et al., 2003; Bowen et al., 2002; Hinds et al., 2003; Renshaw et al., 1986). Strategies to optimize particle incorporation and contrast behavior have been developed by using different lipofection agents (Frank et al., 2003), translocation peptides (Lewin et al., 2000), or by use of phagocytosis only (Moore et al., 1997). Initial studies on the visualization of grafted magnetically labeled cells have been

* Corresponding author. Department of Radiology and Neuroradiology, Charité University Hospital, Schumannstr. 20/21, D-10117 Berlin, Germany.
E-mail address: albrecht.stroh@charite.de (A. Stroh).
[1] Both authors contributed equally to this work.
Available online on ScienceDirect (www.sciencedirect.com).

1053-8119/$ - see front matter © 2004 Elsevier Inc. All rights reserved.
doi:10.1016/j.neuroimage.2004.09.014

conducted both in vitro (de Laquintane et al., 2002) and ex vivo (Bulte et al., 1999; Fleige et al., 2001). These studies showed that neurotransplantation of, for example, magnetically labeled oligodendrocyte progenitors is feasible and that MRI can visualize cell migration and myelination (Bulte et al., 1999). In vivo visualization of labeled cells after transplantation has been shown in other studies in the rat brain (Bulte et al., 2002a,b; Fleige et al., 2001; Modo et al., 2002a) as well as in the swine heart (Hill et al., 2003; Kraitchman et al., 2003). Recently, it was shown in a rat model of ischemia that, after injection of magnetically labeled embryonic stem cells into the nonischemic side of the brain, stem cells migrated along the corpus callosum, populating the border zone of the ischemic area of the contralateral hemisphere (Hoehn et al., 2002). A similar migration behavior was observed after implantation of magnetically labeled bone marrow stromal cells in a rat model with a cortical lesion (Jendelova et al., 2003). The migration velocity of grafted subventricular zone cells, labeled with iron oxide particles, has been measured in a rat stroke model (Zhang et al., 2003). However, in all these studies, large numbers of cells (10^5–10^6) were grafted and observed.

To obtain a detailed insight into migration processes or to observe cells after intravascular administration, it would be advantageous to detect many fewer cells (<1000). The feasibility of observing single cells with MR methods in vitro has been demonstrated very recently (Foster-Gareau et al., 2003; Hinds et al., 2003). For in vivo investigations, however, only rough estimates of the minimum number of detectable cells are available to date.

In our study, we have used a 17.6 T magnet (the highest magnetic field available for MRI of rodents) combined with an efficient cellular magnetic labeling scheme (Fleige et al., 2002). The purpose of the investigation was to explore the limits of MRI detection of grafted cells in the rat brain in vivo.

Materials and methods

Cell culture of embryonic stem cells

Mouse embryonic stem cells (CRL-1934, ATCC, Manassas, USA) were grown in DMEM media (ATCC) containing medium conditioned by feeder cells (CRL-1503, ATCC), 15% fetal calf serum (PAA, Pasching, Austria), 15 ng/ml leucemia inhibitory factor (LIF)(Sigma-Aldrich, Munich, Germany), 0.1 mM 2-mercaptoethanol (Sigma-Aldrich), and 1% penicillin–streptomycin (Sigma-Aldrich). The cells were cultured in 75 cm^2 cell culture flasks (Nunc, Wiesbaden, Germany) with 20-ml medium at 37°C and 5% CO_2 and passaged every 3 days. Only the undifferentiated cells in suspension were used for the experiments. After washing the cells in phosphate-buffered saline (PBS) (Gibco, Invitrogen, Karlsruhe, Germany), they were counted in a Neubauer counting chamber. The viability was determined by staining with trypan-blue solution (0.4%) (Sigma-Aldrich).

Labeling of stem cells with very small superparamagnetic iron oxide particles

For cellular labeling we used very small superparamagnetic iron oxide particles (VSOP) C200 (Ferropharm, Teltow, Germany). VSOP have advantages for in vitro cell labeling compared to ultrasmall superparamagnetic iron oxide particles (USPIO)(Fleige et al., 2002). Although VSOP contain an iron oxide core with a diameter of 5 nm, similar to USPIO, the total particle size is much smaller than the diameter of USPIO particles, which ranges from 20 to 40 nm due to the extended dextran coating. The VSOP are coated by monomer citrate giving a total diameter of 9 nm and a negative surface charge. For fluorescence labeling of VSOP, the fluorescent dye rhodamine green succimidyl ester hydrochloride (Molecular Probes, Eugene, OR) was conjugated with pentaethylene–hexamine. The resulting rhodamine green–pentaethylene–hexamine conjugate was bound by adsorption to the surface of the VSOP nanoparticles. The dispersion of VSOP–rhodamine green was purified by ultrafiltration using a 50-kDa Pellicon-XL filter (Millipore, Billerica, USA). The iron oxide particles were added to the stem cells in the culture flask at a concentration of 1.5 mM and incubated with the cells for 90 min at 37°C and 5% CO_2. No lipofection agent was used during incubation. After incubation, the cells were harvested, centrifuged at 1000 rpm (Labofuge 400R, Heraeus-Sepatech, Osterode, Germany) and washed twice in PBS. The viability was determined by staining with trypan blue, and vital cells were counted in a Neubauer chamber. The respective cell number was adjusted by centrifugation of the cells at 1000 rpm and the uptake of the pellet in the respective volume of PBS.

Determination of the accuracy of the final cell number

In addition to the counting procedure described above, the cell number was confirmed by counting the vital cells in their final concentration by fluorescence microscopy and using a Neubauer chamber. The number of centrifugation steps remained the same in all experiments.

For fluorescence microscopy, 100 μl of cell suspension was incubated with 10 μl of 0.1% ethidium bromide solution (Molecular Probes) and 10 μl of 0.1% acridine orange solution (Molecular Probes) for fluorescence vitality staining. After washing, 2 μl of the cell suspension was pipetted onto a slide and covered with a small coverslip. At a magnification of ×200, the vital cells were counted using an inverse fluorescence microscope (Leica, Heidelberg, Germany). The counting was conducted independently three times for each concentration, and two independent experiments were carried out. The number of vital cells in the Neubauer chamber was determined as described above. Additionally, all concentrations were counted independently three times, with four counts each, giving a total number of 12 counts per concentration.

Relaxometry and atomic absorption spectroscopy (AAS)

After incubating with iron oxide particles and harvesting, the cell number was determined, and the cells were again centrifuged and suspended in medium. Two milliliters of cells was placed into ventilated 14-ml tubes (Falcon, BD Biosciences, San Jose, CA, USA), giving 6×10^5 cells per probe. The control cells were treated in the same way.

The NMR transverse relaxation time (T_2) was measured at 0.49 T by relaxometry (Minispec, Bruker, Ettlingen, Germany).

For atomic absorption spectroscopy (AAS) measurements, 6×10^5 stem cells were resuspended in 2 ml of medium after particle incubation (as described above). One milliliter of 65% HNO_3 (Merck, Darmstadt, Germany) and 10 μl H_2O_2 (Merck-Schuchardt, Hohenbrunn, Germany) were added. The solution was incubated for 24 h to lyse the cells. The disaggregated cells were filtered, and

the iron content was measured by AAS (Solaar, Unicam, Cambridge, UK).

Confocal laser scanning microscopy (CLSM)

The cells were seeded in six-well plates (Falcon, BD Biosciences) at a concentration of 1×10^5 cells/3 ml without LIF. After 24 h, rhodamine green (Molecular Probes)-labeled iron oxide particles (VSOP C200, Ferropharm) were added at a concentration of 1.5 mM, and the adherent cells were incubated for 90 min at 5% CO_2 and 37°C. After incubation for 45 min with the membrane-specific fluorescent dye di-8-ANEPPS (Molecular Probes), cells were washed twice in PBS to remove both fluorescent dye and iron oxide particles which had not been taken up.

The uptake of VSOP by stem cells was visualized using a confocal laser scanning microscope (CLSM) (Leica). The adherent stem cells were observed in six-well plates with a ×20 water immersion objective (NA 0.5, Leica). Fluorescent dyes (rhodamine green and di-8-ANEPPS) were excited simultaneously at a wavelength of 488 nm. Fluorescence from green (rhodamine green) and red (di-8-ANEPPS) channels was collected by two photomultiplier tubes (PMTs) using two filters, 510–560 nm and 610–670 nm, respectively. Data from each channel were merged into final two-color images.

Gel phantoms

For in vitro MR imaging, gel phantoms were prepared by dissolving 1.5 g agar (Qbiogene, Heidelberg, Germany) in 100 ml TAE buffer (Qbiogene). A volume of 12 ml of the heated gel was immediately poured in 15-ml Falcon tubes. The liquid gel was centrifuged at 3000 rpm for 5 min to remove air bubbles. The magnetically labeled embryonic stem cells were resuspended in PBS. The cell number was determined as described above. A Hamilton microsyringe fitted with a 26-gauge blunt needle was used for injection of the stem cells both in vitro and in vivo. Four injections of 2 μl of a cell suspension with a defined cell number were conducted for each gel phantom. After injection, the syringe was slowly retracted, and the gel phantoms were again centrifuged at 800 rpm for 4 min to reduce air bubbles in the needle track.

Stereotactic transplantation of magnetically labeled stem cells

Magnetically labeled embryonic stem cells were suspended in 2 μl PBS after adjustment of the respective cell number. Female Wistar rats (130–150 g) (Charles River WIGA, Sulzfeld, Germany) were anesthetized with isoflurane (Abbott, Wiesbaden, Germany). In deep anesthesia, the rats were placed in a stereotactic frame. Each animal received an injection of 2-μl (1μl/2 min) cell suspension into the striatum of the left brain hemisphere via a Hamilton microsyringe. The needle remained at the location of the injection for 10 min before it was slowly pulled out, in order to reduce the protraction of the cells into the needle track.

A total number of 17 animals were transplanted for MRI. The animals received a transplantation into the left striatum (from bregma: incisor bar −2.4, AP −0.5, ML 4.0, DV −5.0). Out of the 17 animals, 6 received 1000 unlabeled cells and 11 received labeled cells (1 animal, 120,000; 3 animals, 1000; 3 animals, 100; and 4 animals, 20).

Additionally, for the histological quantification of the cell number, six animals were transplanted according to the above described protocol, with three animals receiving 100 and three animals 1000 labeled cells.

MR imaging

MRI was performed on a 750-MHz wide bore MR spectrometer (Bruker, Rheinstetten, Germany) equipped with an animal handling system inside an imaging gradient system with 200-mT/m maximum gradient strength. A linear 38-mm-diameter birdcage resonator was used for transmission and reception. Three or more 3D gradient echo imaging experiments were performed on each animal. One or more low-resolution data sets ($195 \times 390 \times 390$ μm^3, TE/TR = 3.0/20 ms) of the whole brain were acquired in 82 s each to verify parameter settings. A 3D data set with an isotropic resolution of 98 μm was acquired with a $(256)^3$ matrix over a field of view of $(2.5\ cm)^3$ comprising the whole brain; TE/TR = 3.0/20 ms; scan time 22 min. After identification of the transplantation site, a second high-resolution 3D data set with 98-μm isotropic resolution but $256 \times 256 \times 128$ points was recorded over a smaller field of view: TE/TR = 4.6/15 ms; scan time 32 min (four averages). The signal-to-noise ratio (SNR) in the images was between 20 and 30:1 in gray matter regions of the brain. For the animal that had received 120,000 cells, a modified protocol with lower spatial resolution ($117 \times 117 \times 183$ μm^3, TE/TR = 2.7/30 ms) was sufficient to observe the cells. All animals were imaged immediately after transplantation and several animals at different time points up to 4 weeks later.

Gels were imaged with a 3D gradient echo sequence with 98-μm isotropic spatial resolution; $256 \times 256 \times 256$ acquisition matrix; TE/TR = 5/20 ms. The flip angle of the excitation pulse was between 5° and 10° in all experiments yielding images that were strongly T_2^*- and moderately T_1-weighted.

Image processing was performed with the software packages Paravision (Bruker) and Amira (TGS, San Diego, USA).

In order to show that the T_2^* effect due to cell injection correlates to the number of injected cells, the volume of signal void at the transplantation site was determined in the animals that had received 100 and 1000 labeled cells. Pixels displaying signal reduced to the noise level were counted for three animals with 100 and three animals with 1000 cells in the data sets with TE = 3.0 ms, and for two animals with 100 and two animals with 1000 cells in the data sets with TE = 4.6 ms.

Histologic examination

Immediately after the final imaging sessions, rats were euthanized with an overdose of pentobarbital and either perfused for paraffin embedding or prepared for frozen sectioning. The latter was frozen in liquid nitrogen, tissue blocks were mounted in optimal cutting temperature (OCT) compound, and 15-μm and 30-μm (SSEA), respectively, thick serial sections were cut on a Jung cryostat (Leica, Germany). Six animals with survival times of 3 weeks each were perfused with 250 ml of normal saline and then with 250 ml of phosphate-buffered 10% formalin. Of these animals, two had been injected with 1000 unlabeled cells, one with 100 labeled cells, and three with 20 labeled cells. After removal, the brains were stored in formalin. Each brain was later cut into three slices in either the frontal plane parallel to the needle tract or in the horizontal plane perpendicular to the needle tract. The slices were embedded in paraffin, and up to 96 serial sections of 6-μm thickness were cut from the block containing the needle

tract in each animal. Sections were stained with hematoxylin and eosin, Masson, cresyl violet, and Prussian blue for iron. Immunohistochemistry was performed in cases where transplanted cells were observed in conventionally stained slides. Using the ABC method and primary antibodies for MIB (Ki67) (Sigma), PNCA (Sigma), GFAP (Sigma), vimentin (Sigma), synaptophysin (Sigma), neurofilaments (Sigma), and the stem cell antibody SSEA-1 (Sigma), the reaction products were developed with benzidine, and the sections were counterstained with hematoxylin.

In order to determine the actual cell number within the tissue and to obtain information about potential cell loss in the injection device in two animals with 1000 injected cells, a quantitative histological evaluation of 6-μm (Prussian blue) and 25-μm (SSEA) serial sections around the needle track stained for Prussian blue and SSEA was performed. The iron-positive and SSEA-positive stem cells within the tissue were counted, and the distribution of the cells was determined and visualized graphically as a map.

Statistics

Data of the AAS and NMR analysis and of the cell quantifications are shown as mean ± standard deviation (SD). Statistical significance was calculated by an unpaired *t* test, and a value of $P < 0.05$ was considered to be significant.

Results

Intracellular uptake of iron oxide particles by embryonic stem cells

Incubation with 1.5 mM VSOP led to a significant uptake of iron by the stem cells, measured by AAS, as shown in Fig. 1a. Control cells exhibit 0.16 ± 0.02 μg Fe per million cells, whereas cells incubated with 1.5 mM VSOP exhibit 7.1 ± 0.4 μg Fe per million cells. The intracellular iron concentration was increased by a factor of 49, making the incorporated VSOPs responsible for 98% of the total iron in the cell after incubation. Relaxometry measurements of the stem cells in vitro at 0.49 T resulted in T_2 relaxation times of 1516 ± 12 ms for the suspended control cells in comparison to 358 ± 41 ms for the suspended cells incubated with 1.5 mM VSOP (Fig. 1b). These measurements demonstrated a reduction of the T_2 relaxation time by 76% after incubation with VSOP.

To test whether the iron particles are incorporated into the cell or only attached to the cellular surface, we used confocal laser scanning microscopy (CLSM) and fluorescent iron oxide particles. Fig. 2 shows CLSM images of embryonic stem cells incubated with 1.5 mM rhodamine-labeled VSOP and the membrane marker ANEPPS. An overview (Fig. 2a) displays both channels, detecting the fluorescent signal from rhodamine green-labeled VSOP (green color) and ANEPPS (red color), resulting in a yellow signal in the case of colocalization. Several embryonic stem cells are shown; one of them is cut in the middle by the focus plane. Cellular uptake of rhodamine–VSOP is definitively shown by green fluorescence, partly overlaid with the red fluorescence. The homogeneous intensity of the yellow signal indicates that no significant discrepancy between rhodamine–VSOP uptake occurs. In Figs. 2b–d, a cross-section through the middle of a single embryonic stem cell, including the nucleus, is displayed. In the green channel (Fig. 2b), a large signal caused by the fluorescence of the rhodamine-labeled iron oxide particles can be detected, generally

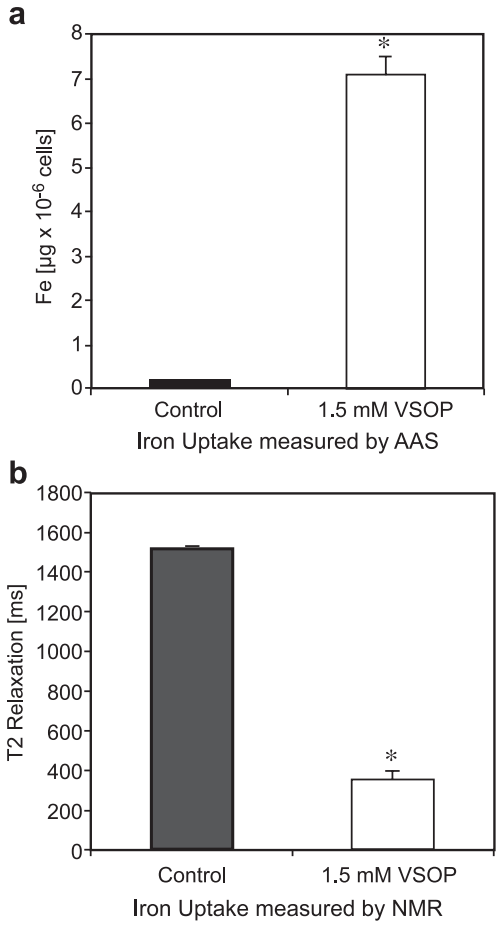

Fig. 1. Measurement of the iron uptake in embryonic stem cells after incubation with VSOP. The iron uptake was monitored directly via AAS and indirectly via the reduction of the NMR T_2 relaxation time. Panel a represents the iron content of the embryonic stem cells after incubation with VSOP determined by Atomic Absorption Spectroscopy (AAS). In panel b, the iron oxide particle uptake is determined by the reduction of the transverse relaxation time T_2. The values represent the mean ± SD of two independent experiments with four measurements each (*$P < 0.05$ control vs. 1.5 mM).

proving the intracellular presence of VSOP. The red channel (Fig. 2c), dominated by the ANEPPS fluorescence, shows the cellular and nuclear membrane as well as intracellular vesicles. The colocalization of the two channels (Fig. 2d) reveals that the VSOP aggregates are surrounded by membranes forming endocytotic vesicles. The latter are clearly located within the cell.

Impact of magnetic labeling on the viability and differentiation potential of embryonic stem cells

Staining with trypan blue after incubation with 1.5 mM VSOP did not reveal a decrease in the vitality rate of the embryonic stem cells compared to controls. The vitality rates were approximately 95% after the last centrifugation step, prior to transplantation. VSOP-labeled stem cells cultured under normal culture conditions in the presence of the differentiation inhibitor LIF did not show any unwanted differentiation. Differentiation of both labeled and nonlabeled embryonic stem cells to the stage of neuronal precursors was conducted according to the five-step protocol developed by Lee et al. (2000). FACS analysis showed equal

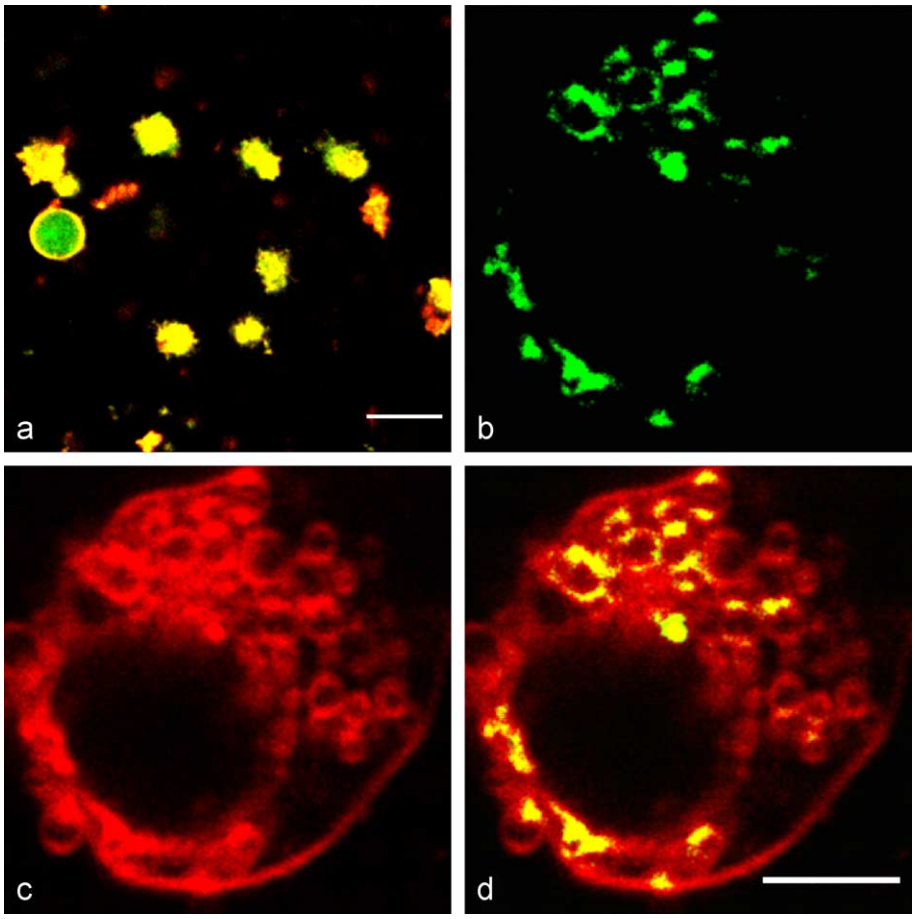

Fig. 2. CLSM images of embryonic stem cells. Two channels were simultaneously recorded during microscopy. Green fluorescence represents VSOP, whereas red fluorescence represents the membrane marker ANEPPS. Panel a represents an overview, displaying both green and red channels. Overlay of green and red fluorescence results in a yellow signal. Scale bar represents 20 μm. Panels b–d show a single embryonic stem cell. Panel b displays the green channel (510–560 nm), panel c represents the red channel (610–670 nm), and panel d shows an overlay of green and red channels, scale bar 5 μm.

numbers of neuronal precursors identified as nestin-positive cells (data not shown).

Accuracy of cell counts

In order to determine the minimum number of detectable cells, the first question was how accurately the cell number can be counted. Table 1 shows the cell numbers counted in samples adjusted to 10, 50, and 500 cells/μl as used in the transplantations. The standard deviation for concentrations of 500 and 50 cells/μl was below 15%. At the lowest concentrations of 10 cells/μl, the standard deviation was around 30–40%. At all three concentrations, no significant difference was found between the number obtained with the Neubauer chamber and the number with fluorescence microscopy.

Table 1
Accuracy of cell counts determined by Neubauer counting chamber and fluorescence microscopy

Adjusted cell number (cells/μl)	Final cell number determined by Neubauer chamber	Final cell number determined by fluorescence microscopy
500	377 ± 52	400 ± 50
50	38 ± 2	46 ± 6
10	9 ± 3	8 ± 3

In vitro MR visualization of cells

In order to assess the potential of gradient echo MR methods in conjunction with our labeling strategy and the transplantation protocol, we injected 2 μl of different concentrations of VSOP-labeled cells into agarose gels according to the in vivo transplantation protocol. In T_2^*-weighted MR images, the gel appeared homogeneous, indicating that it was virtually free from air bubbles. The injection canals were identified by slightly higher signal intensity compared to the gel. Fig. 3 shows longitudinal sections through two (Figs. 3a, c) and three (Fig. 3b) out of four injection canals in the gels for injections of unlabeled (500 cells/μl) and labeled cells (500 and 50 cells/μl), respectively. Labeled cells were detected as areas corresponding to signal reduction in the image along the injection canal. Whereas with 500 cells/μl, large areas of signal loss were observed along the entire canal (Fig. 3b), with 50 cells/μl dark areas were spatially distinct and signal reduction was less pronounced (Fig. 3c). The injection of 1000 unlabeled cells showed no significant areas of signal loss in the injection canal (Fig. 3a).

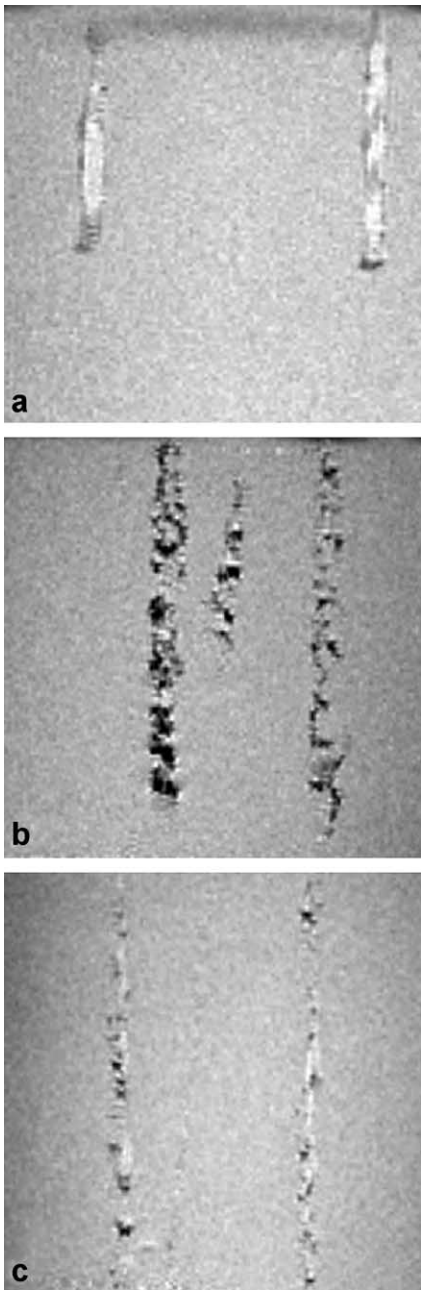

Fig. 3. Gradient echo MR images of gel phantoms after injection of stem cells. (a) Gel with injection of 1000 unlabeled stem cells. The two injection canals show a slightly higher signal intensity than the gel. No cells can be observed. (b) Gel with injection of 1000 VSOP-labeled stem cells. Three injection canals can be seen. Cells are clearly visible as areas of signal loss. (c) Gel with injection of 100 VSOP-labeled stem cells. Cells are clearly visible as small areas of signal loss.

In vivo MRI of labeled cells

In order to explore the minimum number of cells that can be identified by MRI in vivo, we transplanted different numbers of labeled and unlabeled stem cells into the striatum of 17 female Wistar rats. The intrinsic image contrast allowed distinction between gray and white matter structures such as corpus callosum, fornix, and anterior commissure. Parts of the ventricles and vessels could also be identified. In the latter, signal intensity depended strongly on the orientation of blood flow. Transplantation of 120,000 labeled cells was easily identified via large regions of very low intensity (Fig. 4a). Directly after transplantation (approximately 1 h), the cells were distributed throughout a wide area inside the left hemisphere (Fig. 4b). Besides the transplantation canal, cells were distributed over the left ventricle. No cells were observed in the right hemisphere. Three days after transplantation, only minor changes in the cell distribution were observed. The signal loss along the canal was slightly less pronounced, while the distribution in the ventricle was slightly more widespread. In addition to the left ventricle, cells were also observed in the left part of the third ventricle. Over a

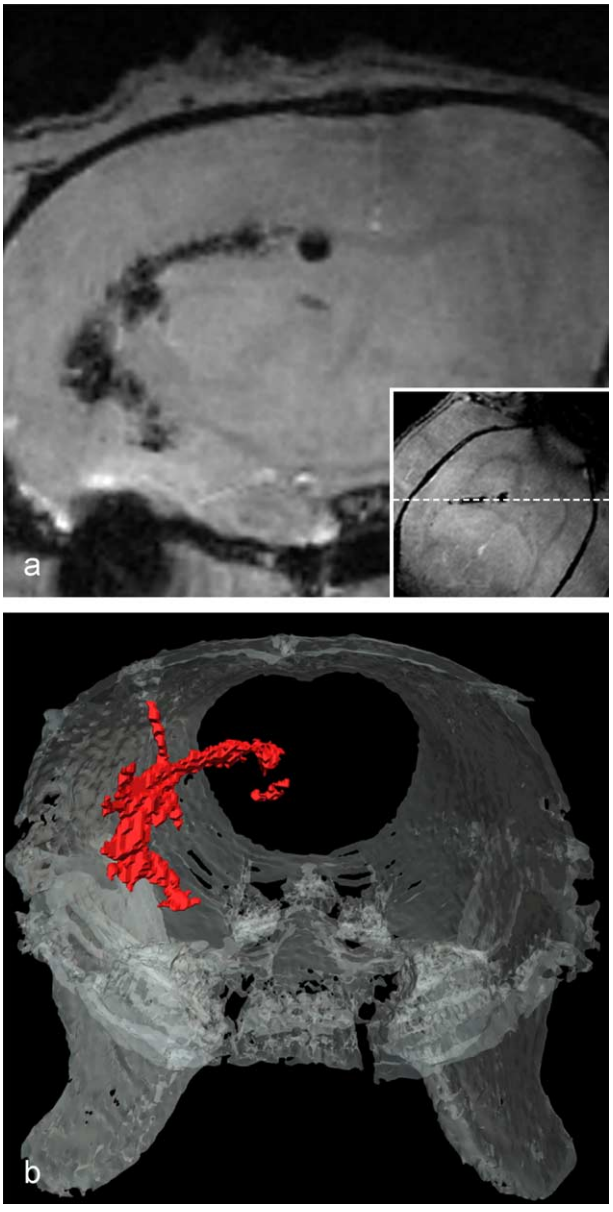

Fig. 4. Transplantation of 120,000 VSOP-labeled stem cells into rat brain. (a) A gradient echo MR image through the brain. Cells are observed as a large dark area. The dashed line in the inset shows the orientation of the imaging slice in a coronal section. (b) Volume rendering of the stem cells (red) in the brain. Part of the skull and jaw bones are shown for orientation.

period of the next 22 days, no significant changes in the location of the cells were found.

After transplantation of 1000 labeled cells in the striatum of three rats, a clearly visible area of signal loss, extending to the deep end of the transplantation canal, was observed in each animal (Fig. 5a). In contrast, none of the six animals that had 1000 unlabeled cells transplanted into them showed a comparable signal loss at the transplantation site (Fig. 5b). Nevertheless, in two animals, significant signal losses in the upper part of the needle track were observed, which resulted from a small hemorrhage, detected on histology (data not shown). Transplantation of 100 cells resulted in an area of signal extinction which was easily visible in several slices of the 3D data set (Fig. 6a), but the area of signal loss became smaller. A distribution along the canal that may have resulted from retraction of the needle was also visible (dotted arrow). In Fig. 6a, several smaller areas of signal loss are seen in the deeper part of the brain (solid arrow). Infiltration of CSF or microbleeding that can cause similar signal extinction would be observed as larger, contiguous areas. After transplantation of approximately 20 cells, only small areas of reduced signal were observed, extending only over two or three slices in the data sets (data not shown). However, the small dimension and the incomplete loss of the signal did not allow the attribution of these observations unambiguously to the labeled cells. Here, infiltration of CSF or blood may have been the cause of the signal loss. Also, some anatomical structures display similar regions of low signal in the images. Fig. 6b of a control animal shows the normal anatomical structures with, for example, a hypointense signal along some of the vessels (arrows).

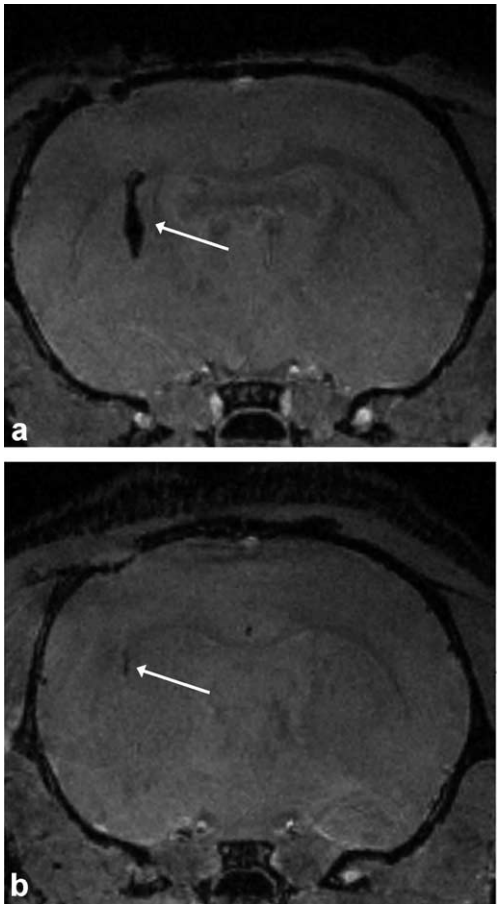

Fig. 5. MR images of the rat brain after transplantation of 1000 VSOP-labeled (b) and unlabeled (b) stem cells. Labeled cells are clearly seen as a large dark area at the transplantation site. Unlabeled cells only caused minor signal changes in the transplantation canal.

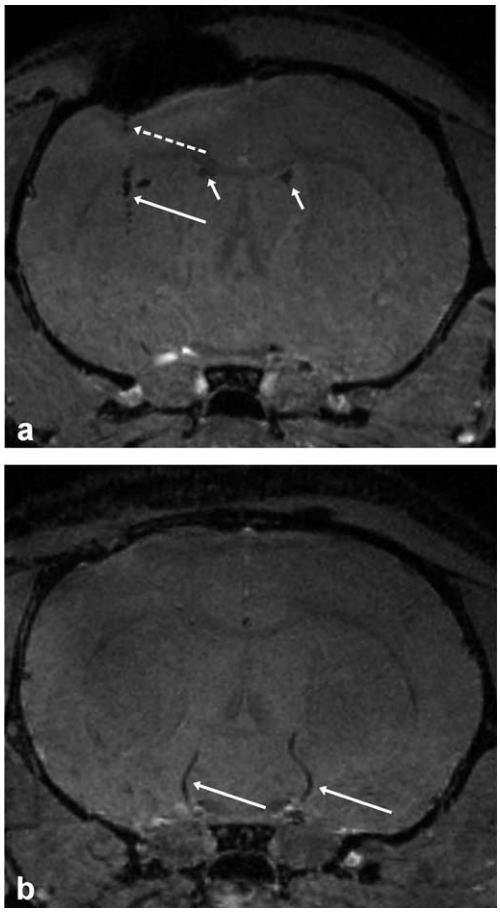

Fig. 6. MR images of the rat brain after transplantation of 100 VSOP-labeled stem cells compared to a control animal. In panel a, clusters of small numbers of cells are seen along the canal. The lateral ventricles are also observed as areas of low signal (short arrows). Panel b shows a section distant from the transplantation site from a data set of a rat that had received unlabeled cells.

An estimate of the dependence of T_2^* on the number of transplanted cells was not possible, since the signal was reduced to the noise level in the hypointense areas at the shortest achievable TE of 3.0 ms. The T_2^* effects in the images, manifested as the extent of the signal void, showed an increase with both the number of transplanted cells and TE. After transplantation of 100 cells, signal voids of 183 ± 86 pixels and 204 ± 132 pixels were found and, after transplantation of 1000 cells, voids of 492 ± 135 pixels and 654 ± 86 pixels, for TE = 3.0 ms and TE = 4.6 ms, respectively. This provides an empirical quantification of the T_2^* effects that are, in our experimental setup, about a factor of three more pronounced after transplantation of 1000 cells compared to 100 cells. The large variation between individual animals, and therefore large standard deviation in the reported numbers, results from variations in the local cell density at the transplantation site and thus renders a more rigorous quantification unfeasible.

Histology and histological quantification of transplanted embryonic stem cells

Histologically, the needle tract was found in all perfused animals after careful scrutiny of serial sections in both horizontal and frontal brain cuts. The few sections containing the tract showed a small cortical glial scar, sometimes with a tiny central defect. Figs. 7a–c represent the same animal 3 weeks after cell transplantation. Fig. 7a shows a coronal section of an animal injected with 1000 labeled cells. The needle tract (arrow) passes from the left parietal cortex through the corpus callosum, showing a small hemorrhage in the basal ganglia. These small microbleedings could be seen both within and in the vicinity of the needle tract in some animals, including the two control animal which exhibited contiguous hypointense signal changes in the MR images. In animals injected with 100 and 20 cells, only single cells positive for iron (Prussian blue staining) or the stem cell marker SSEA could be found. In animals injected with 1000 labeled cells, a significant number of iron-positive cells lying in the lower portion of the needle tract were found (Fig. 7b). Fig. 7c shows the quantitative histological evaluation of the 14 (out of a total of 33) serial sections positive for Prussian blue from the same animal. The distribution of the 832 stem cells within the needle tract (green) and in the immediate vicinity to the left and right of it is schematically indicated in 1-mm distances from the surface. No stem cells were present within 1 mm of the surface, and a larger portion was dispersed within the immediately adjacent callosal fibers. Fig. 7d is from a different animal; here, the brain has been removed at the transplantation day. The figure displays a coronal section of 25-μm thickness including a total number of 60 cells positive for the embryonic stem cell marker SSEA (brown staining product) in the needle track. Counting of SSEA-positive cells in 10 serial sections of the needle track and close vicinity revealed a total of 746 SSEA-positive cells. No SSEA-positive cells were found in different areas of the brain.

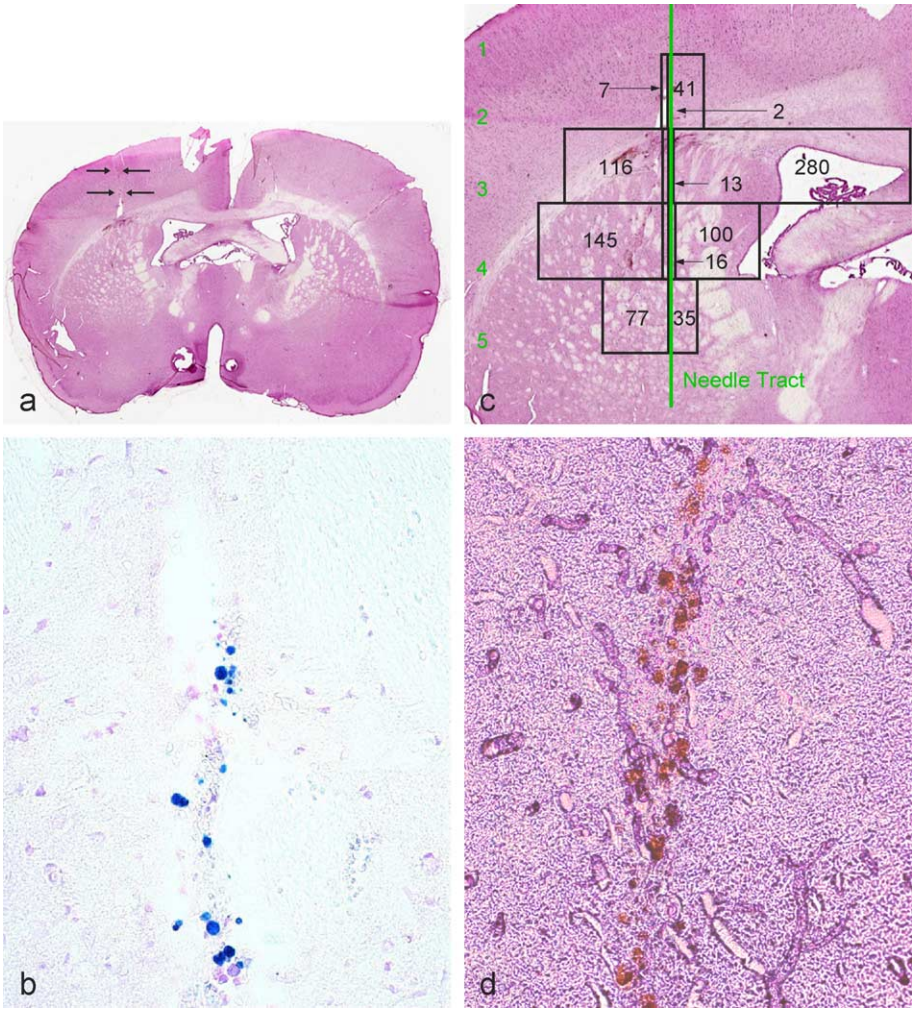

Fig. 7. Histology of a rat after transplantation of 1000 VSOP-labeled stem cells. (a) Coronal section of rat brain after stereotactic implantation of 1000 stem cells. The needle tract is marked by arrows. (Frozen section, hematoxylin, and eosin). (b) Serial section stained with Prussian blue for iron and counterstained with fast red. Groups of iron-positive stem cells can be seen mainly within the needle tract. (c) Schematic figure of the quantitative histological evaluation of Prussian blue-positive stem cells. Altogether, 832 stem cells could be counted within and in the neighborhood of the upper part (1-mm distances from the surface) of needle tract (green). A larger portion could be found within and below the adjacent callosal fibers. (d) Serial section of 25-μm thickness stained for SSEA. (Frozen section, SSEA 1 immunohistochemistry, hematoxylin counterstaining.) A total number of 60 SSEA-positive cells (brown staining product) can be seen within the needle tract. Different animal as a–c, implantation of 1000 stem cells.

In one long-term survival animal injected with 1000 non-labeled cells, a conspicuous cellular conglomerate of approximately 1-mm diameter was present at the end of the needle tract in the subcortical white matter, suggestive of neoplasia. At higher magnification, this circumscribed lesion contained a polymorphous population of cells. There was regional heterogeneity with either small undifferentiated and densely packed cells, or larger cells of epithelial appearance with nuclear hyperchromasia and mitoses. Perivascular rosettes and also true rosettes of the Flexner type were seen in several places. These cells were positive for GFAP and showed a high proliferation index using the MIB antibody (not shown).

Discussion

In this study, we have shown that VSOP are incorporated by mouse embryonic stem cells in sufficient amounts to act as an efficient cellular label. This supports results from previous studies (Fleige et al., 2002; Stroh et al., 2004) that VSOP are suitable labels with low side effects on cell populations. Both AAS and relaxometry measurements show a very large uptake of iron oxide particles by embryonic stem cells. Relaxometry measurements have been shown to be a quick and effective tool for the semiquantitative measurement of iron oxide particle concentration by the reduction in the T_2 relaxation time. Compared to AAS, relaxometry is considerably less time-consuming. CLSM data support the notion that VSOP, coated with monomer citrate, are incorporated by stem cells via endocytosis, similar to a previously demonstrated uptake of dextran-coated iron oxide particles (Fleige et al., 2001; Moore et al., 1997). The particles form aggregates surrounded by membranes, which prevent direct contact between the VSOP and the cytosol. Our MRI results show that a single incubation step with VSOP is sufficient for in vivo detection of labeled stem cells. Several different labeling strategies have already been established, which make use of, for example, lipofection (Frank et al., 2003) or translocation peptides (Lewin et al., 2000). The question, however, of whether such procedures result in an increased sensitivity of the MR experiments or whether they in fact harm the cells has not yet been answered. For example, a recent study showed that magnetic labeling leads to an increase of cellular oxidative stress. However, the increase seemed to be transient, and no long-term effects regarding cellular proliferation and viability were found (Stroh et al., 2004). Further systematic studies addressing possible effects of the labeling procedure on differentiation and migration of the cells are clearly required.

The first prerequisite for the determination of the minimum detectable cell number is a reliable method for controlling the number of cells. Comparison with fluorescence microscopy demonstrated that our procedure is accurate, keeping in mind the high dilution of the cells. Even in the case of the highest dilution of only 10 cells/μl, the standard deviation is within an acceptable range. The results of the counting procedure suggest that the concentration is slightly overestimated, due to an inevitable loss of cells in the last centrifugation step.

In vitro MRI experiments showed that cells labeled with VSOP can be visualized in T_2^*-weighted images after injection into agarose gels. We estimate that less than 10 cells are sufficient to be observed in vitro. The possibility of visualizing single labeled cells with gradient echo imaging methods at very high magnetic fields has recently been shown for cells labeled with larger iron particles (Hinds et al., 2003).

Our in vivo data clearly show that 1000 grafted and magnetically labeled cells are observed at the transplantation site as a large area of low signal. No corresponding signal attenuation is found with unlabeled cells. In two control animals, a high degree of signal loss was observed only in the upper canal in an area contiguous to the surface of the skull, histologically verified as small microhemorrhages. Apart from these two animals, only very small signal alterations were observed in the control animals. Areas of signal void were smaller in the animals that had received 100 labeled cells compared to animals that had received 1000 labeled cells but were still significantly greater than the small signal changes found in the controls. In two animals that received 10 cells/μl, a small region of reduced signal in the injection canal was clearly identified. However, it cannot be excluded that this signal reduction is caused by infiltration of CSF or blood. Histological quantifications of the cell number revealed that 832 cells stained for Prussian blue and 746 cells stained for SSEA could be found at the transplantation site in animals with (nominally) 1000 transplanted cells. These numbers are in accordance with the in vitro quantification. The lower number of SSEA-positive cells is probably due to the antibody not binding all of the stem cells present in the tissue compared to the very robust Prussian blue staining. Furthermore, the histology shows that the MR hypointensities are unambiguously caused by VSOP-containing stem cells as both iron- and SSEA-positive cells were found in the direct vicinity of the needle track. In animals with only 100 or 20 grafted cells, it was not possible to locate reliably the cells in the tissue sections. This is not surprising keeping in mind that the histological slice thickness is between 6 and 25 μm compared to the diameter of the needle track of 200 μm and the volume of the transplanted cell suspension of 2 μl.

We have performed our investigation at the highest magnetic field available for imaging of rodents, 17.6 T. Higher magnetic fields have two major benefits: first, a higher equilibrium magnetization gives a higher intrinsic image SNR. Second, differences in the magnetic susceptibility, introduced by the iron particles in the grafted cells, lead to much more pronounced signal reductions than at lower field strengths. Thus, at 17.6 T, comparable contrast is observed with far fewer cells than at lower fields. If the goal is to observe the bulk motion of several thousands of cells, low magnetic field strengths are sufficient. But, if the focus is on the microscopic migration and distribution of small numbers of cells, such as studying stem cell recruitment after stroke (Modo et al., 2002b), high magnetic fields are necessary.

One potential method to increase further the sensitivity to T_2^* effects is the use of steady-state free-precession (SSFP) sequences. These have recently been shown to enable detection of single iron-labeled cells, embedded in a gel, at 1.5 T (Foster-Gareau et al., 2003). However, SSFP sequences are extremely prone to image artifacts in inhomogeneous media, or if the object is moving. The sensitivity towards artifacts increases with the strength of the magnetic field. Only recently have SSFP sequences produced images of fixed samples at 11.75 T superior in contrast-to-noise to conventional gradient echo methods (Kohler et al., 2003). High field applications of SSFP sequences on living animals remain extremely problematic and have, to the best of our knowledge, not been reported to date.

Summarizing our results, approximately 100 cells are clearly observable by high-resolution MRI and can be distinguished from other sources of signal reduction. Numbers as low as 20 cells and below are potentially detectable in animals in vivo under optimized experimental conditions. The dominant problem at these low cell numbers is the distinction of cells and other sources of contrast (mainly microhemorrhages induced through the implantation). However, in the monitoring of stem cells in different animal models, the problem of induced microhemorrhages will be of less relevance, since cells are often not grafted directly at the lesion site. Time course studies of animals will also facilitate the distinction between hemorrhages and cells migrating towards the lesion sites.

Acknowledgments

The authors thank F. Marschinke, K. Hild, B. Hamm, and J. Schnorr for support; K. Kraemer, I. Schimpke, and S. Außenhofer for excellent technical assistance and help with image processing and quantification; A. Wizenmann for access to her cell culture facilities. Financial support was given by the Deutsche Forschungsgemeinschaft (Ha1232/13), the Alexander von Humboldt Stiftung, and the Bundesministerium für Bildung und Forschung (BMBF).

References

Arbab, A.S., Bashaw, L.A., Miller, B.R., Jordan, E.K., Bulte, J.W., Frank, J.A., 2003. Intracytoplasmic tagging of cells with ferumoxides and transfection agent for cellular magnetic resonance imaging after cell transplantation: methods and techniques. Transplantation 76, 1123–1130.

Ben Hur, T., Einstein, O., Mizrachi-Kol, R., Ben Menachem, O., Reinhartz, E., Karussis, D., Abramsky, O., 2003. Transplanted multipotential neural precursor cells migrate into the inflamed white matter in response to experimental autoimmune encephalomyelitis. Glia 41, 73–80.

Bjorklund, L.M., Sanchez-Pernaute, R., Chung, S., Andersson, T., Chen, I.Y., McNaught, K.S., Brownell, A.L., Jenkins, B.G., Wahlestedt, C., Kim, K.S., Isacson, O., 2002. Embryonic stem cells develop into functional dopaminergic neurons after transplantation in a Parkinson rat model. Proc. Natl. Acad. Sci. U. S. A. 99, 2344–2349.

Bowen, C.V., Zhang, X., Saab, G., Gareau, P.J., Rutt, B.K., 2002. Application of the static dephasing regime theory to superparamagnetic iron-oxide loaded cells. Magn. Reson. Med. 48, 52–61.

Bulte, J.W., Zhang, S., van Gelderen, P., Herynek, V., Jordan, E.K., Duncan, I.D., Frank, J.A., 1999. Neurotransplantation of magnetically labeled oligodendrocyte progenitors: magnetic resonance tracking of cell migration and myelination. Proc. Natl. Acad. Sci. U. S. A. 96, 15256–15261.

Bulte, J.W., Douglas, T., Witwer, B., Zhang, S.C., Lewis, B.K., van Gelderen, P., Zywicke, H., Duncan, I.D., Frank, J.A., 2002a. Monitoring stem cell therapy in vivo using magnetodendrimers as a new class of cellular MR contrast agents. Acad. Radiol. 9 (Suppl. 2), S332–S335.

Bulte, J.W., Duncan, I.D., Frank, J.A., 2002b. In vivo magnetic resonance tracking of magnetically labeled cells after transplantation. J. Cereb. Blood Flow Metab. 22, 899–907.

Bulte, J.W., Ben Hur, T., Miller, B.R., Mizrachi-Kol, R., Einstein, O., Reinhartz, E., Zywicke, H.A., Douglas, T., Frank, J.A., 2003. MR microscopy of magnetically labeled neurospheres transplanted into the Lewis EAE rat brain. Magn. Reson. Med. 50, 201–205.

Check, E., 2003. Parkinson's transplant therapy faces setback. Nature 424, 987.

de Laquintane, B.D., Dousset, V., Solanilla, A., Petry, K.G., Ripoche, J., 2002. Iron particle labeling of haematopoietic progenitor cells: an in vitro study. Biosci. Rep. 22, 549–554.

Eskandar, E.N., Flaherty, A., Cosgrove, G.R., Shinobu, L.A., Barker, F.G., 2003. Surgery for Parkinson disease in the United States, 1996 to 2000: practice patterns, short-term outcomes, and hospital charges in a nationwide sample. J. Neurosurg. 99, 863–871.

Fleige, G., Nolte, C., Synowitz, M., Seeberger, F., Kettenmann, H., Zimmer, C., 2001. Magnetic labeling of activated microglia in experimental gliomas. Neoplasia 3, 489–499.

Fleige, G., Seeberger, F., Laux, D., Kresse, M., Taupitz, M., Pilgrimm, H., Zimmer, C., 2002. In vitro characterization of two different ultrasmall iron oxide particles for magnetic resonance cell tracking. Invest. Radiol. 37, 482–488.

Foster-Gareau, P., Heyn, C., Alejski, A., Rutt, B.K., 2003. Imaging single mammalian cells with a 1.5 T clinical MRI scanner. Magn. Reson. Med. 49, 968–971.

Frank, J.A., Miller, B.R., Arbab, A.S., Zywicke, H.A., Jordan, E.K., Lewis, B.K., Bryant Jr., L.H., Bulte, J.W., 2003. Clinically applicable labeling of mammalian and stem cells by combining superparamagnetic iron oxides and transfection agents. Radiology 228, 480–487.

Fukunaga, A., Uchida, K., Hara, K., Kuroshima, Y., Kawase, T., 1999. Differentiation and angiogenesis of central nervous system stem cells implanted with mesenchyme into ischemic rat brain. Cell Transplant 8, 435–441.

Hill, J.M., Dick, A.J., Raman, V.K., Thompson, R.B., Yu, Z.X., Hinds, K.A., Pessanha, B.S., Guttman, M.A., Varney, T.R., Martin, B.J., Dunbar, C.E., McVeigh, E.R., Lederman, R.J., 2003. Serial cardiac magnetic resonance imaging of injected mesenchymal stem cells. Circulation 108, 1009–1014.

Hinds, K.A., Hill, J.M., Shapiro, E.M., Laukkanen, M.O., Silva, A.C., Combs, C.A., Varney, T.R., Balaban, R.S., Koretsky, A.P., Dunbar, C.E., 2003. Highly efficient endosomal labeling of progenitor and stem cells with large magnetic particles allows magnetic resonance imaging of single cells. Blood 102, 867–872.

Hoehn, M., Kustermann, E., Blunk, J., Wiedermann, D., Trapp, T., Wecker, S., Focking, M., Arnold, H., Hescheler, J., Fleischmann, B.K., Schwindt, W., Buhrle, C., 2002. Monitoring of implanted stem cell migration in vivo: a highly resolved in vivo magnetic resonance imaging investigation of experimental stroke in rat. Proc. Natl. Acad. Sci. U. S. A. 99, 16267–16272.

Isacson, O., Bjorklund, L.M., Schumacher, J.M., 2003. Toward full restoration of synaptic and terminal function of the dopaminergic system in Parkinson's disease by stem cells. Ann. Neurol. 53 (Suppl. 3), S135–S146.

Jendelova, P., Herynek, V., DeCroos, J., Glogarova, K., Andersson, B., Hajek, M., Sykova, E., 2003. Imaging the fate of implanted bone marrow stromal cells labeled with superparamagnetic nanoparticles. Magn. Reson. Med. 50, 767–776.

Kohler, S., Hiller, K.H., Griswold, M., Bauer, W.R., Haase, A., Jakob, P.M., 2003. NMR-microscopy with TrueFISP at 11.75T. J. Magn. Reson. 161, 252–257.

Kraitchman, D.L., Heldman, A.W., Atalar, E., Amado, L.C., Martin, B.J., Pittenger, M.F., Hare, J.M., Bulte, J.W., 2003. In vivo magnetic resonance imaging of mesenchymal stem cells in myocardial infarction. Circulation 107, 2290–2293.

Lee, S.H., Lumelsky, N., Studer, L., Auerbach, J.M., McKay, R.D., 2000. Efficient generation of midbrain and hindbrain neurons from mouse embryonic stem cells. Nat. Biotechnol. 18, 675–679.

Lewin, M., Carlesso, N., Tung, C.H., Tang, X.W., Cory, D., Scadden, D.T., Weissleder, R., 2000. Tat peptide-derivatized magnetic nanoparticles allow in vivo tracking and recovery of progenitor cells. Nat. Biotechnol. 18, 410–414.

Lindvall, O., Sawle, G., Widner, H., Rothwell, J.C., Bjorklund, A., Brooks, D., Brundin, P., Frackowiak, R., Marsden, C.D., Odin, P., 1994. Evidence for long-term survival and function of dopaminergic grafts in progressive Parkinson's disease. Ann. Neurol. 35, 172–180.

Modo, M., Cash, D., Mellodew, K., Williams, S.C., Fraser, S.E., Meade, T.J., Price, J., Hodges, H., 2002a. Tracking transplanted stem cell migration using bifunctional, contrast agent-enhanced, magnetic resonance imaging. NeuroImage 17, 803–811.

Modo, M., Rezaie, P., Heuschling, P., Patel, S., Male, D.K., Hodges, H., 2002b. Transplantation of neural stem cells in a rat model of stroke: assessment of short-term graft survival and acute host immunological response. Brain Res. 958, 70–82.

Moore, A., Weissleder, R., Bogdanov Jr., A., 1997. Uptake of dextran-coated monocrystalline iron oxides in tumor cells and macrophages. J. Magn. Reson. Imaging 7, 1140–1145.

Pluchino, S., Quattrini, A., Brambilla, E., Gritti, A., Salani, G., Dina, G., Galli, R., Del Carro, U., Amadio, S., Bergami, A., Furlan, R., Comi, G., Vescovi, A.L., Martino, G., 2003. Injection of adult neurospheres induces recovery in a chronic model of multiple sclerosis. Nature 422, 688–694.

Renshaw, P.F., Owen, C.S., McLaughlin, A.C., Frey, T.G., Leigh Jr., J.S., 1986. Ferromagnetic contrast agents: a new approach. Magn. Reson. Med. 3, 217–225.

Stroh, A., Zimmer, C., Gutzeit, C., Jakstadt, M., Marschinke, F., Jung, T., Pilgrimm, H., Grune, T., 2004. Iron oxide particles for molecular magnetic resonance imaging cause transient oxidative stress in rat macrophages. Free Radical Biol. Med. 36, 976–984.

Sun, Z.H., Lai, Y.L., Zeng, W.W., Zhao, D., Ye, Z.W., Zuo, H.C., Xie, Z.P., 2003. Mesencephalic progenitors can improve rotational behavior and reconstruct nigrostriatal pathway in PD rats. Acta Neurochir. (Suppl. 87), 175–180.

Zhang, Z.G., Jiang, Q., Zhang, R., Zhang, L., Wang, L., Zhang, L., Arniego, P., Ho, K.L., Chopp, M., 2003. Magnetic resonance imaging and neurosphere therapy of stroke in rat. Ann. Neurol. 53, 259–263.